

Low Froude Number stratified flows interacting with an isolated obstacle

Jorge A. Gutiérrez¹ and Alan J. Thorpe

*Joint Centre for Mesoscale Meteorology, Department of Meteorology,
University of Reading, England*

(Recibido 1 octubre 1997, aceptado 2 diciembre 1997)

ABSTRACT

In previous studies it has been postulated that vortices, which are observed in the lee of mesoscale mountains, may be due to a variety of interactions of the upstream flow with the mountain including the inviscid baroclinic production of vorticity, the influence of the Earth's rotation and the role of frictional processes in the boundary layer.

Here the relative importance of these three mechanisms is quantified for an upstream flow, with constant static stability, past a mountain with dimensions such that the Rossby number is 0.4 and the Froude number is 0.2. A simple Ekman-type boundary layer is used for simulations in which the role of friction is calculated. The full vorticity budget is evaluated so that the dominant sources of vorticity can be found from the numerical simulations, which use a non-hydrostatic, three-dimensional model. It is found that if a frictional boundary layer is included the lee vortices are formed at the flanks of the orography due to viscous mechanisms. The (inviscid) baroclinic mechanism exists but is a small contribution. The asymmetry introduced by the Earth's rotation accentuates the tendency for shedding of the lee vortices.

The frictional effects also act as a source of potential vorticity. However caution needs to be applied when interpreting the potential vorticity budget because there is a source due to the implicit numerical dissipation inherent in this, and any other model. This implicit source makes the dynamical interpretation of the so-called inviscid simulations in potential vorticity terms difficult if not impossible. For such problems the use of vorticity, rather than potential vorticity thinking is less ambiguous.

The production of vorticity and potential vorticity is studied in a low Froude number stratified flow over and around an isolated bell-shaped mountain with a circular base. The effects of background rotation and surface friction have been considered. Without background rotation and shear and using a free-slip lower boundary condition for inviscid flow the baroclinic mechanism is the main source of horizontal vorticity. This

¹ Corresponding author address: Dr. Jorge A. Gutiérrez, Laboratorio de Investigaciones Atmosféricas y Planetarias, y Centro de Investigaciones Geofísicas, Escuela de Física, Universidad de Costa Rica, 2060 San José, Costa Rica. E-mail: jgutier@titan.efis.ucr.ac.cr

horizontal vorticity is tilted into the vertical and generates two counter-rotating lee-vortices. With background rotation the baroclinic mechanism remains an important source of horizontal vorticity but it is closely followed by additional tilting terms which depend on the Coriolis parameter.

Simulations of viscous flow using a no-slip boundary condition show that the baroclinic term is then not an important contributor to the horizontal vorticity budget. Much larger values of vertical vorticity are found on the upwind side of the orography than in the other two cases, due to the tilting of the horizontal vortex tubes created by the no-slip boundary condition.

A quantity called normalised potential vorticity is defined to allow the relation between the amount of vorticity and potential vorticity being produced to be quantified. It is produced from early in the integration for both non-rotating and rotating inviscid flows, due to the implicit diffusion implied by the numerical method. In the viscous flow more normalised potential vorticity is produced due to the inclusion of friction. For a easterly flow in the northern hemisphere, negative potential vorticity is produced on the northern flank of the orography and positive potential vorticity is produced on the southern flank. The onset of vortex shedding due to asymmetries in the flow is also studied. The asymmetries were introduced by including background rotation creating an asymmetry in the upwind flow allowing the lee eddies to be shed.

1. Introduction

The study of the generation and shedding of lee-vortices is a very interesting and challenging problem. Several observed flow features induced by highly complex topography, such as the Denver cyclone have been related to the vortex shedding mechanism. Circulations like this are sometimes associated with severe weather and have been shown to have a pronounced impact in the air quality of the surrounding area.

The sources of vorticity that lead to lee vortex formation and the mechanisms that cause vortex shedding as well as those that inhibit the shedding of lee-vortices have been the object of intense research during recent years. The mechanisms proposed to explain the generation of vorticity when air moves around orography have been discussed for flows which are inviscid, Smolarkiewicz and Rotunno (1989) or at most pseudo-inviscid, Smith (1989). We present here results on the dynamics of inviscid and viscous flows that point to the possibility that the inviscid mechanisms may have a negligible impact on the dynamics of viscous flows. This is an important result since viscous mechanisms are dominant in the real lower troposphere.

Smith (1989) has proposed a number of mechanisms in order to explain the generation of potential vorticity in inviscid runs. We present a novel way of investigating potential vorticity production in both inviscid and viscous runs, namely by computing the evolution in time of a

normalised potential vorticity and comparing it with the evolution of the vertical vorticity field. Our research also deals with the impact of viscous mechanisms on the shedding of vortices. Grubisic et al (1995) have considered this but they used a shallow water model to perform their calculations. To the best of our knowledge, this is the first time that this important question has been considered using a non-linear, non-hydrostatic model in a stratified atmosphere.

Research on lee vortex formation can be traced back to 1939 when Lettau suggested, after studying surface pressure observations, that vortices were shed in the leeward side of islands. Direct confirmation of this hypothesis took place twenty years later when the first observations from meteorological satellites were made, Hubert and Kruger (1962), Chopra and Hubert (1965).

Smolarkiewicz and Rotunno (1989) proposed an inviscid mechanism of vortex formation in stratified flow. They studied inviscid low Froude number flows without background rotation and found that horizontal vorticity could be produced by the deformation of the isentropes on the upstream side of the orography. The basic flow was unshered and since it was not subjected to the effects of background rotation the only way horizontal vorticity could be produced was through the baroclinic mechanism. This horizontal vorticity would be tilted in the vertical when the flow passed over and around the orography and vertical vorticity would thus be produced. Another interesting feature of their 1989 paper is that

Smolarkiewicz and Rotunno claimed that no potential vorticity was produced in their simulations.

Smith (1989a) commented that the simulations performed by Smolarkiewicz and Rotunno could not be completely free of dissipation due to the fact that all numerical models possess internal dissipation which is used to control the growth of subgrid scale noise. He also mentioned that overturning and turbulence may take place in the flow thus creating potential vorticity, hereafter referred to as PV .

Smith has pointed out that little is known about the process of PV generation at the lower boundary in stratified flows and uses two physically plausible mechanisms that could continue to operate in the inviscid nondiffusive limit. In the first one Smith remarks that as long as the solid boundary remains a density surface, viscous forces tangent to the boundary generate no PV . Aloft, buoyancy vorticity vectors lie tangent to the density surfaces, again giving no PV . When a stagnation point forms and density surfaces intersect the hill, a no-slip condition at the boundary forces the generation of PV . A second possible mechanism of PV production proposed by Smith is related to overturning in a stratified fluid. If fluid overturning and turbulence occur, the cascade of energy to small scales destroys the identity of fluid parcels, and PV is no longer conserved, even in the inviscid nondiffusive limit.

Schär and Smith (1993a) presented results of shallow water flow past isolated topography. Their simulations dealt with inviscid flow with no background rotation. Their main objective was to study the sources of vorticity in shallow water flow. They observed that the production of vorticity is associated with the presence of hydraulic jumps located at the flanks of the orography. At the hydraulic jump the flow is described as pseudo-inviscid because even though there is no explicit viscosity present in the simulations the flow is turbulent at the hydraulic jump and potential vorticity is produced. This potential vorticity is the cause of lee-vortex formation. A left-right symmetry condition was

forced upon the flow in the wake to guarantee the absence of lee-vortex shedding. In another contribution, Schär and Smith (1993b), pointed out that the potential vorticity anomalies created by the hydraulic jumps make the flow potentially susceptible to barotropic instabilities. When the symmetry condition is eliminated the wake becomes elongated with reverse flow, which allows for an instability that breaks the left-right symmetry of the problem. The authors show that the non-linear evolution of this instability breaks up the steady wake into an oscillating von Kármán vortex street.

The influence of asymmetries in the flow on the generation of vortex shedding has been studied by Sun and Chern (1994). They studied inviscid stratified flow interacting with an obstacle whose base is elliptical. Their results show that background rotation, asymmetries in the orography such as different slopes on the flanks of the mountain, and the position of the semi-major axis of the orography with respect to the incoming flow allow the shedding of lee vortices.

The generation of potential vorticity anomalies in flow past orography has been studied by Thorpe et al. (1993), who predicted that in the presence of a boundary layer interacting with orography two areas of potential vorticity production would form on the flanks of the mountain. For a westerly flow in the northern hemisphere an area of negative potential vorticity production on the northern flank of the orography and an area of positive potential vorticity production on the southern flank of the orography. Their results were obtained for a regime whose Froude number is equal to unity, they included background rotation and no lee-vortex formation took place.

The effects of friction on the structure and stability of lee vortices in shallow water flow were studied by Grubisic, Smith and Schär (1995), who found that bottom friction acted in their simulations as an inhibitor of vortex shedding and used this result to explain the apparent quasi-stability of the lee vortices past the island of Hawaii which had been discovered by Smith and

Grubisic (1993) from aerial observations of Hawaii's wake.

All of these studies have not provided a detailed vorticity and potential vorticity budget. This has led to a set of vorticity production mechanisms being proposed but no attempt to compare these quantitatively has been made. It is the aim of this paper to provide this quantitative assessment so that the most important sources and sinks of vorticity and potential vorticity can be found.

2. Numerical model

The numerical model used in this study is a three-dimensional implementation of the dry, non-hydrostatic equation set of Miller and White (1984) in terrain-following σ coordinates developed at the University of Reading by P. Miranda. The model uses radiation boundary conditions at the lateral boundaries and an absorption layer at the top boundary in order to eliminate the possible reflection of vertically propagating waves. The absorption layer consists of a set of model levels where, at each time step Rayleigh damping towards a reference state is applied. To minimise reflection, the time scale of the damping is decreased smoothly through the absorption layer. The equations are integrated using a standard second-order accurate leapfrog numerical scheme. A spatial fourth-order filter has been used to eliminate subgrid scale waves and a time filter has been used in order to eliminate numerical instability. The filtering is done as a sequence of two fourth order filters: first a two-dimensional horizontal filter and then a one-dimensional vertical filter. The equations of the model are described in Miranda and James (1992).

In all the simulations described in this paper the obstacle used is a bell-shaped mountain having the form:

$$z(x, y) = \frac{h}{\left[1 + \left(\frac{x - x_o}{a}\right)^2 + \left(\frac{y - y_o}{b}\right)^2\right]^{\frac{3}{2}}} \quad (1)$$

where h is the maximum height of the obstacle and a and b are the half-width lengths of the mountain in the x and y directions respectively. In all the computations shown in this paper h has a value of 2 km and $a = b = 50$ km which means that the mountain has a circular base. The background flow has a speed of 4ms^{-1} and the background stratification is $N = 10^{-2}\text{s}^{-1}$, where N is the Brunt-Vaisala frequency. The Froude number, $Fr = U/Nh$ has then a value of 0.2, that is, we investigate a low Froude number regime. Unless stated otherwise, the separation between consecutive grid points in both the zonal and meridional directions is equal to 15 km. Thirty levels have been used in the vertical equally spaced in σ (normalised pressure). The model is started impulsively with the upstream flow and the stratification imposed everywhere in the domain.

3. Simulation results

3.1 First case study: Viscous flow with background rotation and surface friction

Here the interaction between viscous flow and orography is investigated. To this effect the parametrisation of a boundary layer with a constant eddy viscosity coefficient has been introduced. The value of the eddy viscosity coefficient has been chosen to be equal to $K = 5\text{m}^2\text{s}^{-1}$. This yields a boundary layer whose depth is a fraction of the mountain height.

The flow profile used to initialise the simulation is an Ekman-type profile that corresponds to such an eddy viscosity coefficient. This yields a boundary layer depth of about one kilometre, that is, half the mountain height. A no-

slip lower boundary condition has been implemented and the temperature field has not been subjected to diffusion. Thus, far away from the mountain the flow behaves as an Ekman type flow.

Vertical and horizontal filters are not used since the explicit diffusion that has been introduced is capable of eliminating the subgrid scale noise. The simulation takes place on an f -plane located at 40 degrees north of the equator.

A numerical experiment was performed where viscous flow was allowed to move on a flat surface with a no-slip lower boundary condition. The flow was found to be balanced and no instabilities were observed. Thus the phenomena observed when viscous flow impinges on an isolated mountain are due entirely to the interaction between the flow and the orography.

Westerly flow impinges on the mountain; an integration of 12 hours shows that an anticyclonic vortex has been formed on the northern flank of the orography. The wind vector field at the surface obtained after an integration of 12 hours is shown on Fig.1. A weak return flow is observed on the lee of the mountain.

The vertical vorticity field at a height of 400 metres above level terrain, which corresponds to about a fifth of the maximum height of the mountain is shown on Fig.2. In analysing these

results it is important to bear in mind that the lee 'rotates' with height since the incoming flow veers with height. One major difference between this vorticity field and the vorticity fields commonly shown in the literature as being the product of inviscid simulations with or without background rotation is the location of the vorticity extrema. In our viscous flow simulation and at a height of 400 metres above level ground the vorticity extrema are located on the flanks of the orography and not on the lee of the obstacle. This indicates that the viscous generation of ζ is dominant over the generation of ζ via stretching of vertically oriented vortex tubes in the lee of the orography.

In order to investigate the sources of vorticity in this simulation we shall consider the different terms of the vorticity equation. We use height coordinates rather than σ coordinates in the analysis of the vorticity equation because it is easier to picture the tilting and stretching mechanisms over flat surfaces rather than on σ surfaces. The vorticity equation may be derived by taking the curl of Boussinesq's momentum equations, when that calculation is performed for the general case with background rotation and viscous forces the following set of equations is obtained:

$$\frac{D\xi}{Dt} - \xi \frac{\partial u}{\partial x} - \eta \frac{\partial u}{\partial y} - \zeta \frac{\partial u}{\partial z} + (\vec{\nabla} \cdot \vec{V})\xi - \frac{\partial b'}{\partial y} - f \frac{\partial u}{\partial z} + \left(\frac{\partial F_z}{\partial y} - \frac{\partial F_y}{\partial z} \right) = 0 \quad (2)$$

$$\frac{D\eta}{Dt} - \xi \frac{\partial v}{\partial x} - \eta \frac{\partial v}{\partial y} - \zeta \frac{\partial v}{\partial z} + (\vec{\nabla} \cdot \vec{V})\eta + \frac{\partial b'}{\partial x} - f \frac{\partial v}{\partial z} + \left(\frac{\partial F_x}{\partial z} - \frac{\partial F_z}{\partial x} \right) = 0 \quad (3)$$

$$\frac{D\zeta}{Dt} - \xi \frac{\partial w}{\partial x} - \eta \frac{\partial w}{\partial y} - \zeta \frac{\partial w}{\partial z} + (\vec{\nabla} \cdot \vec{V})\zeta + f \left(\frac{\partial u}{\partial x} + \frac{\partial v}{\partial y} \right) + \left(\frac{\partial F_y}{\partial x} - \frac{\partial F_x}{\partial y} \right) = 0 \quad (4)$$

where:

$\vec{V} = u\vec{i} + v\vec{j} + w\vec{k}$ and $\vec{F} = F_x\vec{i} + F_y\vec{j} + F_z\vec{k}$ are respectively the wind field vector and the viscous force in component form, f represents the Coriolis

parameter and $b' = g\theta'/\theta_0$ is the buoyancy. The vorticity ω can be expressed as:

$$\vec{\omega} = \vec{\nabla} \times \vec{V} = \xi \vec{i} + \eta \vec{j} + \zeta \vec{k} .$$

Wind vectors on the first sigma level above the surface, T=12 hours

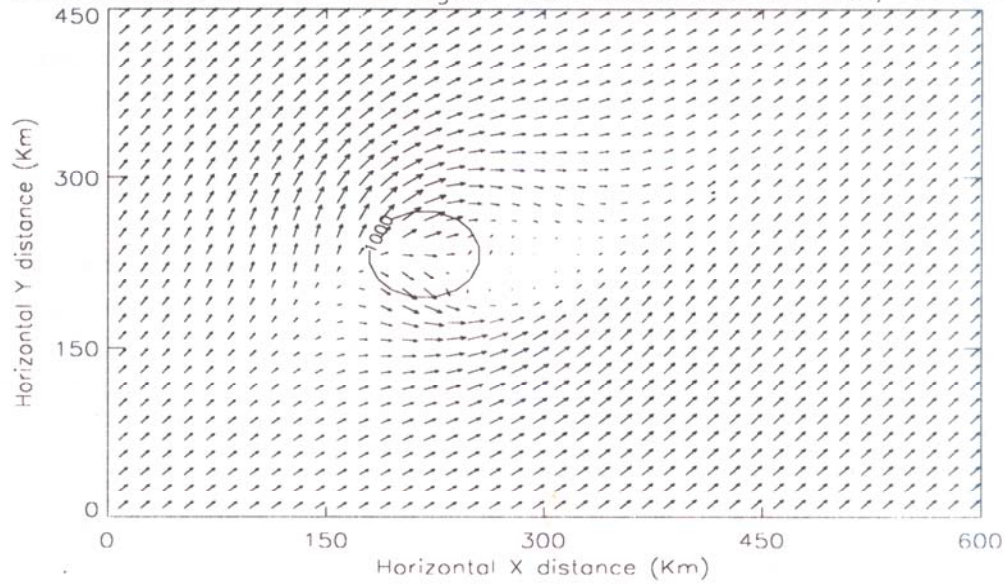


Fig. 1. Wind vectors on the first level above the surface. Viscous flow. Integration time 12 hours. The 1000 metres height contour is shown on the figure. Note that to scale the vectors the upstream flow is 2 ms⁻¹.

REL. VORT. AT Z=400M,T=12hrs,B.L.

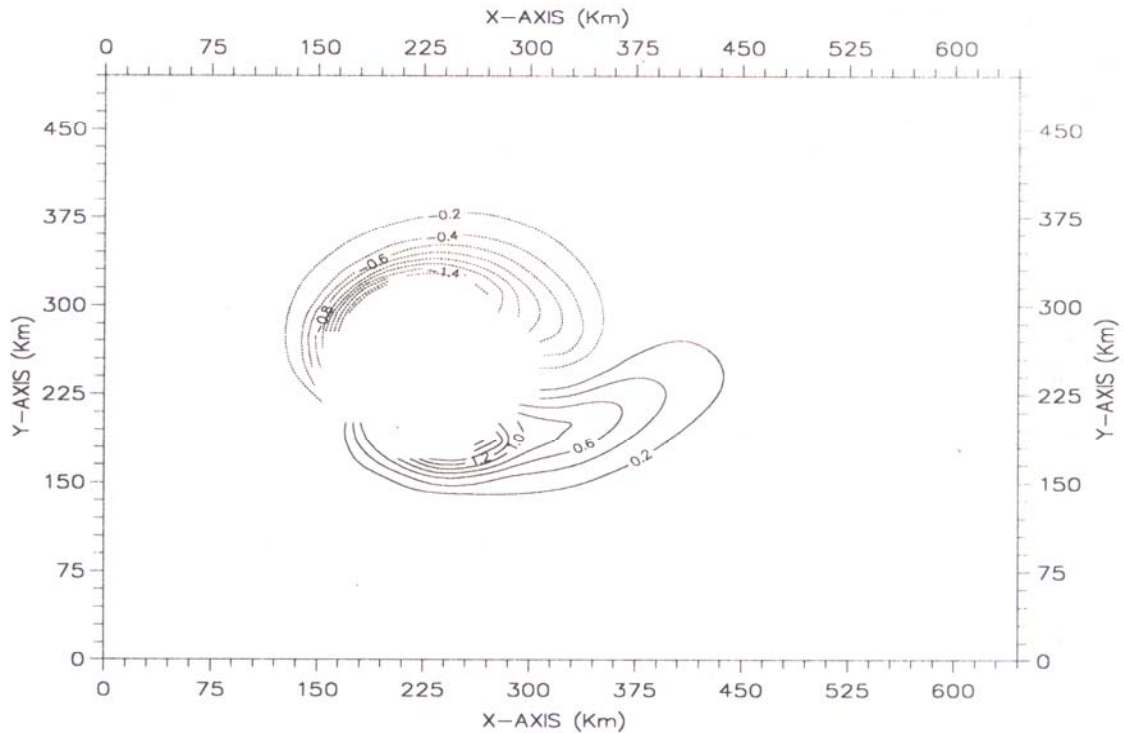


Fig 2: Vertical vorticity field at a height of 400 metres above level ground. Viscous flow with background rotation. Contour interval $0.2 \times 10^{-4} \text{s}^{-1}$. Integration time 12 hours.

In this paper vectors are represented by arrows over the characters.

Horizontal vorticity and the baroclinic term

When the relative contributions to the total vorticity budget are computed it is found that the baroclinic mechanism (e.g., $-\partial b'/\partial y$) is not the leading source of horizontal vorticity. Other vorticity production terms such as, $\eta \partial u/\partial y$, $\zeta \partial u/\partial z$ and $f \partial u/\partial z$ are five times larger than the baroclinic term. This is due to the large shear exhibited by the upstream flow due to the no-slip boundary condition and the large values of ξ , η and ζ generated by the viscous mechanism. This leads to the possibility that even though the baroclinic mechanism is responsible for vortex formation in inviscid low Froude number flows it may not play an important role in the production of vorticity in the real lower troposphere when compared to the contributions from other terms that depend on the vertical shear of the wind field.

Vortex shedding

A calculation of 72 hours shows that no vortex shedding has taken place at a height of 400 metres above level ground. Hence, even though there is background rotation and the upstream flow is not symmetric, conditions shown to lead to vortex shedding by Sun and Chern (1994), the lee vortices remain steady at this level. This agrees with the results of Grubisic et al. (1995), who performed simulations with a shallow water model in which they had included the effects of surface friction. They explained in this way why the lee vortices observed Smith (1993) in Hawaii show no tendency to shed. Nevertheless, calculations of ζ with the Reading Model at higher levels in the flow, for example at 1500 m shown in figure 3, show that vortex shedding takes place at these heights. This is due to the vertical variation of the local Froude number.

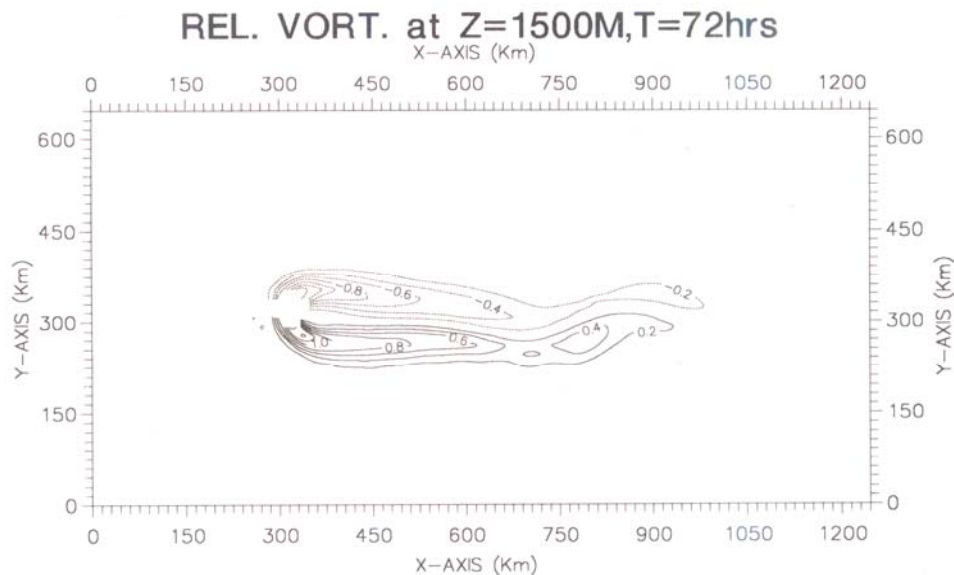


Fig. 3: Vertical vorticity field at a height of 1500 metres above level ground. Viscous flow with background rotation $0.2 \times 10^{-4} \text{s}^{-1}$. Contour interval. Integration time 72 hours.

Vertical structure of ζ

Large values of ζ are found at low levels on the upwind side of the orography. A relative maximum of ζ is located on the lee of the obstacle and ζ decreases rapidly with height. Most of ζ is located within the boundary layer.

A vertical profile of ζ , not shown, shows that, close to the centre of the northern vortex, the intensity of ζ first increases with height up to a height of 500 metres and decreases beyond this height. The initial increase of the absolute value of ζ with height may be attributed to the 'turning' of the lee-vortex with height, since the direction of the upstream flow varies with height due to the fact that the upcoming flow corresponds to an Ekman-type of flow having an eddy viscosity coefficient $K = 5m^2 s^{-1}$.

A calculation of potential vorticity at a

height of 400 metres shows a negative PV anomaly located on the northern flank of the orography, this is shown in Fig.4. The potential vorticity was computed as defined by,

$$PV = \rho^{-1} \vec{\omega} \cdot \vec{\nabla} \theta \quad (5)$$

The structure in Fig. 4 agrees with the results of Thorpe et al. (1993) who obtained a similar pattern when investigating the flow of air parallel to the Alps and discovered negative PV anomalies when analysing atmospheric data, even though their research was done on a $Fr = 1$ flow regime, a different orography was used, and vortex formation was not observed. Nevertheless, it seems that the impact of viscous processes is such as to extend across several flow regimes with different Froude numbers. This mechanism may be important as a source of low level PV anomalies.

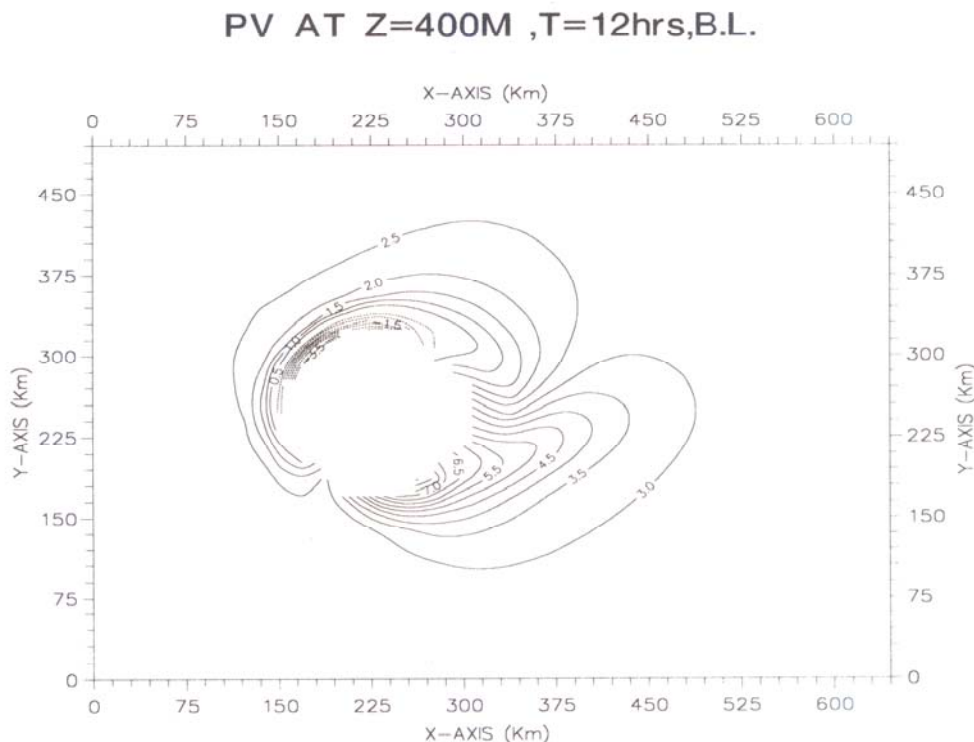


Fig. 4: Potential vorticity at 400 metres above level ground. Viscous flow with no-slip condition. Integration time 12 hours. Contour interval $0.5 \times 10^{-7} m^2 Ks^{-1} kg^{-1}$.

$D(PV)/DT$ AT $Z=400M, T=12hrs$

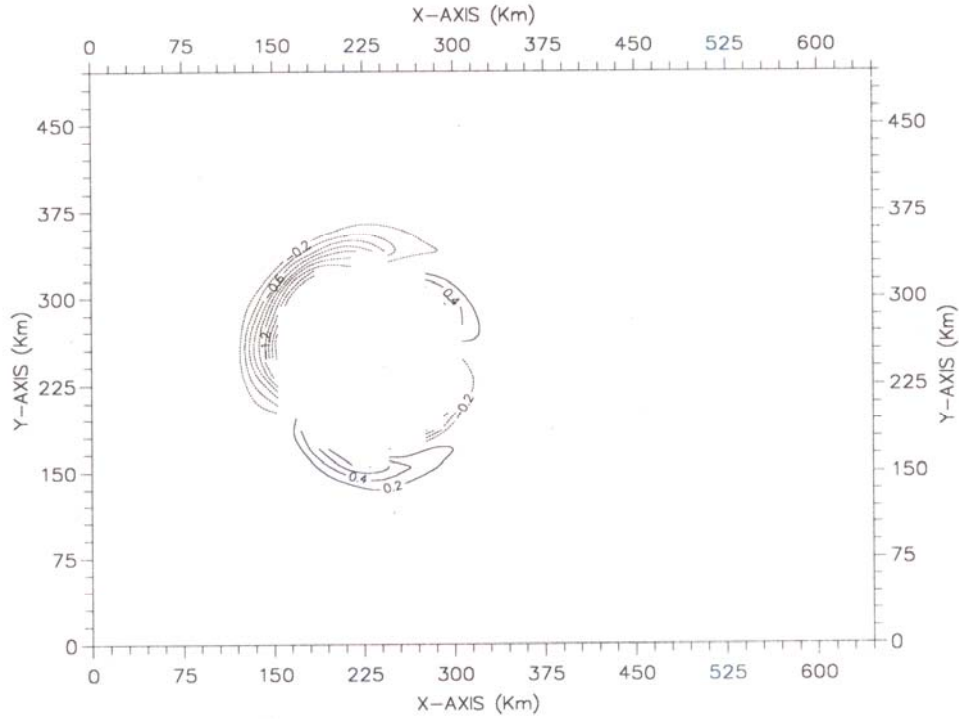


Fig. 5: Rate of production of potential vorticity. The calculation was made for a height of 400 metres above level ground. Viscous flow. Integration time 12 hours. Contour interval $0.2 \times 10^{-10} \text{m}^2 \text{Ks}^{-2} \text{kg}^{-1}$.

Rate of PV production

The evolution of potential vorticity is given by the equation

$$\frac{D(PV)}{Dt} = \rho^{-1} \left[\vec{\nabla} \theta \bullet \vec{\nabla} \times \vec{F} + \vec{\omega} \bullet \vec{\nabla} \theta \right] \quad (6)$$

where \vec{F} represents viscous forces and θ represents the contribution from diabatic source terms. In this simulation $\theta = 0$.

Two main areas of PV production have been found, these can be seen in Fig.5. There is an area of negative PV production located on the northern flank of the orography and an area of positive PV production situated on the southern flank of the orography. The existence of these two areas was predicted by Thorpe et al. (1993) and it can be explained as been due to the sloping of the boundary layer due to the presence of the

orography. There are two small areas of potential vorticity production on the lee of the mountain; these are due to the return flow created by the lee-vortex.

Evolution of PV_{norm} and ζ

Two questions arise: How does the potential vorticity evolve? Is its evolution somewhat related to the evolution of ζ ? In order to answer these questions and be able to compare the evolution of PV and ζ a new quantity will be defined, called normalised potential vorticity, PV_{norm} where:

$$PV_{norm} = \frac{\rho_o PV}{\frac{\partial \theta_{back}}{\partial z}} \quad (7)$$

Where ρ_0 is constant. The physical interpretation of PV_{norm} is that it is the absolute vorticity the air would have if the static stability were to be equal to a reference constant static stability, $\partial\theta_{back}/\partial z$. This is in accord with Rossby's original definition of potential vorticity. Notice that PV_{norm} and ζ have the same units which facilitates comparison of these two fields.

The evolution of PV_{norm} , ζ_{abs} and ζ has been investigated and is shown in Fig.6. There are 12 data points for each field in this figure. The data shown correspond to the extreme values of the fields at a height of 400 metres above level ground. It is found that PV_{norm} values exceed those of ζ_{abs} during the first 12 hours of simulation. This is to be expected since PV_{norm} is

been produced by the dissipative mechanisms that have been introduced in the flow.

3.2 Second case study: Inviscid flow with background rotation

For comparison, to more easily isolate the effects of friction and rotation, we now investigate an inviscid westerly flow, with a free-slip lower boundary condition, that impinges on an isolated bell-shaped mountain with the same dimensions of the orography used in the previous section. Comparison with the previous results highlights the role of surface friction.

Evolution of vertical vorticity, absolute vorticity and PV_{norm} .

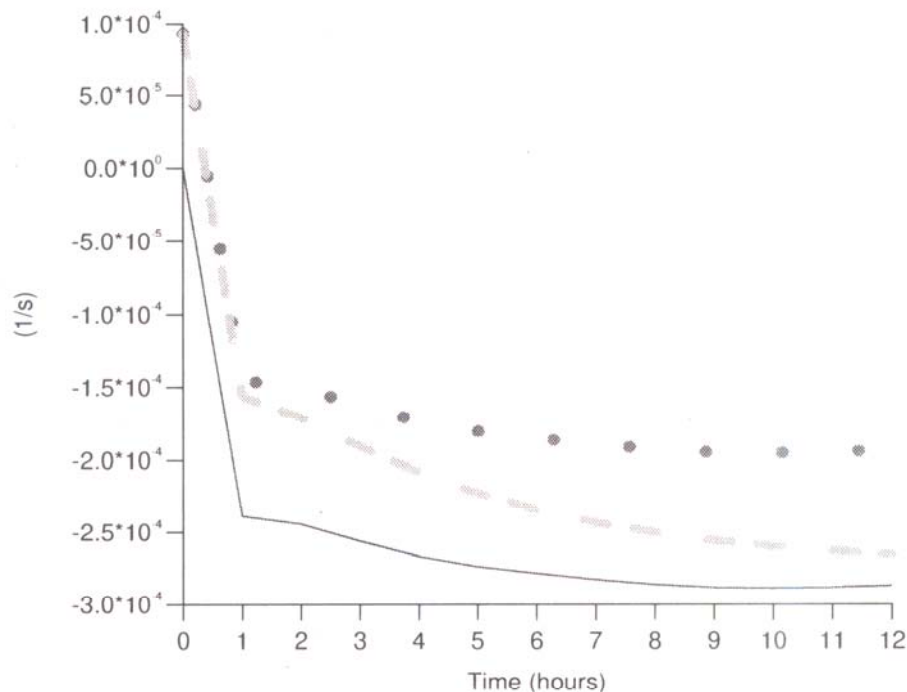


Fig 6: Evolution of ζ (dotted line), ζ_{abs} (continuous line) and PV_{norm} (broken line). Viscous flow with background rotation. Integration time 12 hours.

The surface wind vectors are shown in Fig.7 where the most striking feature is the lack of symmetry caused by the inclusion of rotational effects. A very strong anticyclonic vortex can be

seen on the northern part of the wake and the southern vortex is much weaker than the northern one, this is due to the background rotation of the system. A calculation of ζ shown in Fig.8 shows

that the vorticity field is not symmetric. The vorticity field is stronger here due to the absence of the boundary layer and the new lower boundary condition.

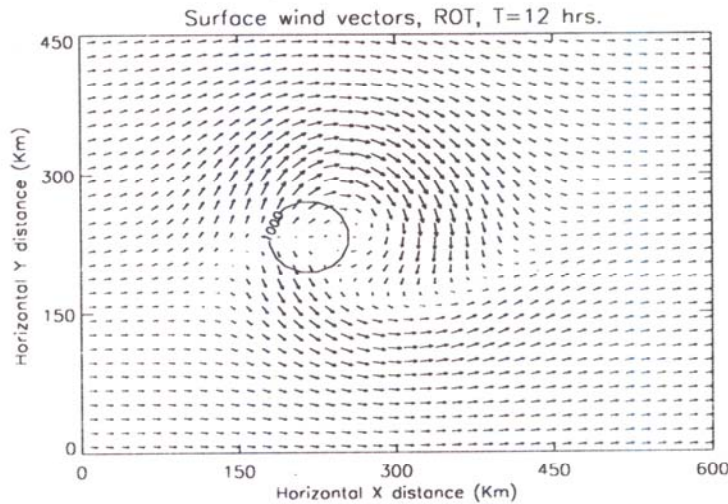


Fig. 7: Surface wind vectors. Inviscid flow with background rotation. Integration time 12 hours. The 1000 metres height contour is shown on the figure. Note that to scale the vectors the upstream flow is 4 ms^{-1} .

REL. VORT. at Z=400M,T=12hrs,ROT

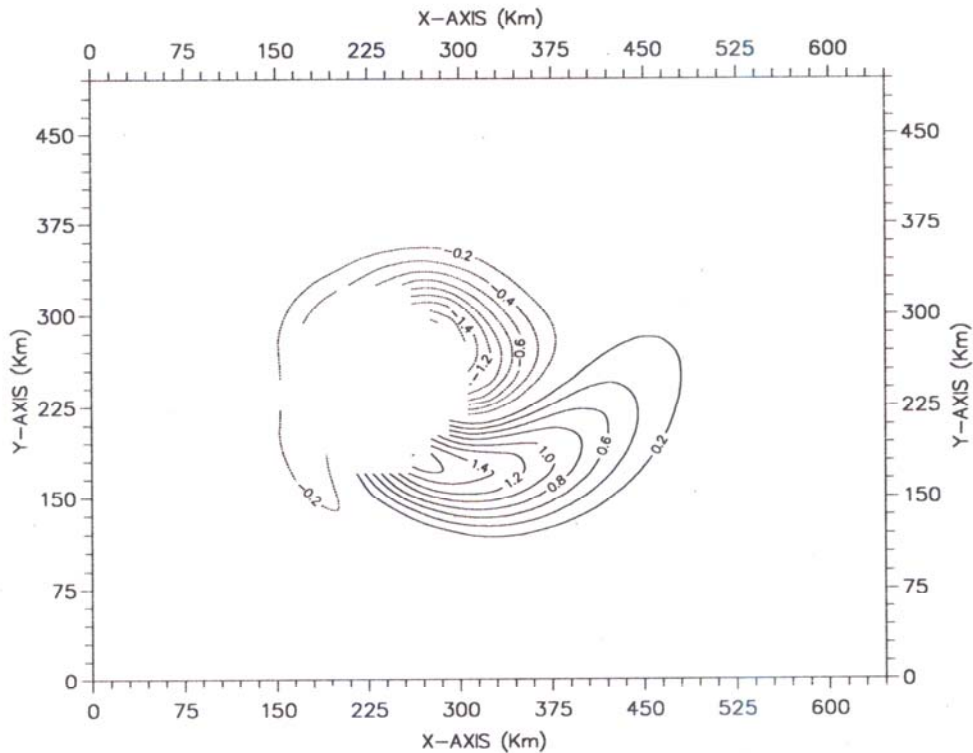


Fig. 8: Relative vorticity field at a height of 400 metres above level ground. Inviscid flow with background rotation. Integration time 12 hours. Contour interval $0.2 \times 10^{-4} \text{ s}^{-1}$.

PV AT Z=400M,T=12hrs,ROT

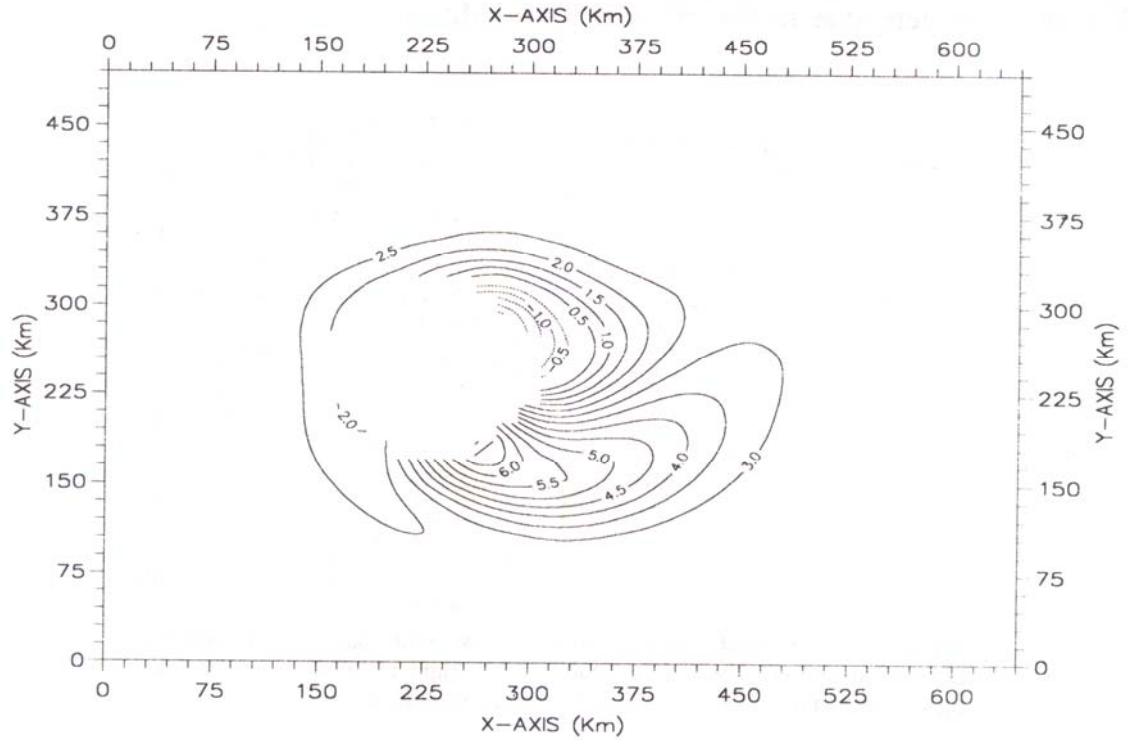


Fig 9: Potential vorticity field at a height of 400 metres above level ground. Inviscid flow with background rotation. Integration time 12 hours. Contour interval $0.5 \times 10^{-7} \text{m}^2 \text{Ks}^{-1} \text{kg}^{-1}$.

Evolution of vorticity, absolute vorticity and PVnorm

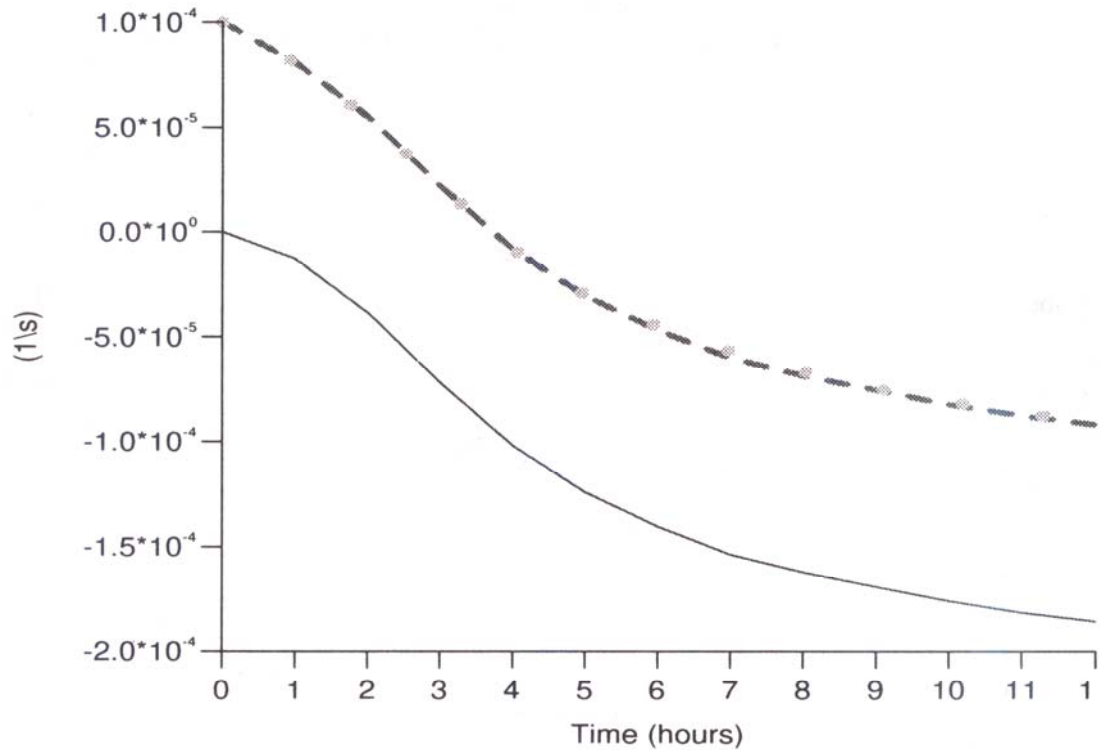


Fig. 10: Evolution of ζ (broken line), PV_{norm} (dotted line) and ζ_{abs} (continuous line). Inviscid flow with background rotation. Integration time 12 hours.

A calculation of potential vorticity at a height of 400 metres above level ground is shown in Fig.9. It can be seen there that potential vorticity has also been generated in this simulation even though it is an inviscid calculation and one would have expected the potential vorticity to be conserved and equal to $2.7 \times 10^{-7} m^2 Ks^{-1} kg^{-1}$.

Thus, some kind of viscous process must be taking place. A possible explanation of the generation of PV in this simulation is the presence of a hydraulic jump. It has been proposed by Smith (1989) that hydraulic jumps may occur at the flanks of the orography and would produce PV that in turn would be responsible for the generation of vorticity in the flow. In order to see if this is the source of the PV found in this calculation the area from 30 km to the south of the southern flank of the mountain up to 30 km to the north of the northern flank of the orography has been scanned in search of evidence of a hydraulic jump by looking at cross sections of the isentropes, but no evidence of a hydraulic jump was found. The only possible cause of the PV observed is the implicit diffusion of the model. Even though this experiment was planned to simulate inviscid flow, spatial filtering has been applied in order to avoid the build up of subgrid scale waves, which lead to the onset of non-linear instability.

The evolution of $PVnorm$, ζ and the absolute vertical vorticity is shown on Fig.10. $PVnorm$ and ζ follow the same evolution in time, but the pattern of $PVnorm$ is different from the one obtained in the first experiment due to the absence of the boundary layer. Schär and Durran (1996) have also observed the production of potential vorticity in *inviscid* simulations.

Vortex shedding

As Sun and Chern (1994) have shown, the breaking of the symmetry of the upstream flow due to the inclusion of background rotation allows the shedding of vortices to take place. An integration of 72 hours shows three main vortex centres have been shed, they can be seen in Fig.11. The domain shown in Fig.11 consists of 83 grid points in the west-east direction and 43 grid points in the north-south direction. This bigger domain was selected in order to study the far-field behaviour, the orography employed in this simulation is the same used in all the numerical experiments discussed here.

The total surface pressure drag exerted by the flow on the orography has been evaluated as:

$$\bar{D} = (D_x, D_y) = \int_{-\infty}^{+\infty} \int_{-\infty}^{+\infty} p_{surface} \bar{\nabla} h(x, y) dx dy \quad (8)$$

where $h(x, y)$ represents the orography.

A calculation of the y-component of the drag shown in Fig.12 shows that the shedding of vortices produces weak oscillations in this component of the drag. The x-component of the drag reaches a steady-state after 16 hours and seems not to be affected by the shedding of lee vortices. The results of this calculation for the viscous flow and for the inviscid flow without background rotation are different and show that both the x and y components of the surface pressure drag quickly reach a steady state.

The long simulation time required to see the shedding of the lee vortices may be due to the fact that the background rotation acts as a very small perturbation to the flow. Perhaps if the flow were perturbed in a more drastic way a higher frequency of vortex shedding could be obtained.

It is found in calculations of westerly flow past a mountain having the same height as the one used in the previous experiment and the same Froude number but a Rossby number equal to 0.8 the frequency of vortex shedding is larger than in the flow having a Rossby number equal to 0.4.

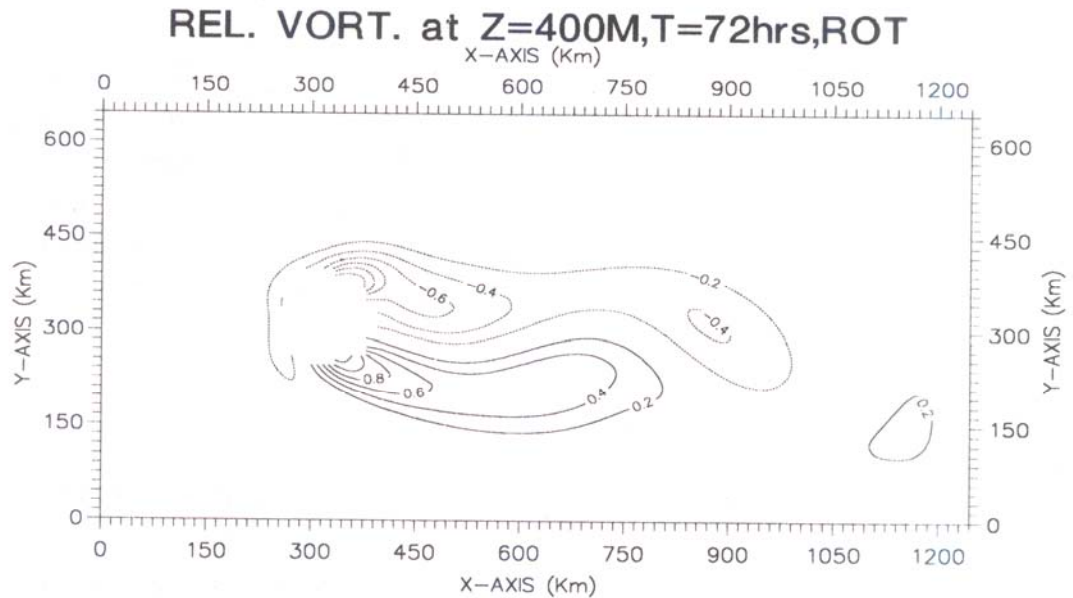


Fig. 11: Vertical vorticity at a height of 400 metres above level ground. Inviscid flow with background rotation. Integration time 72 hours. Contour interval $0.2 \times 10^{-4} \text{s}^{-1}$, $Ro=0.4$.

Evolution of the surface pressure drag

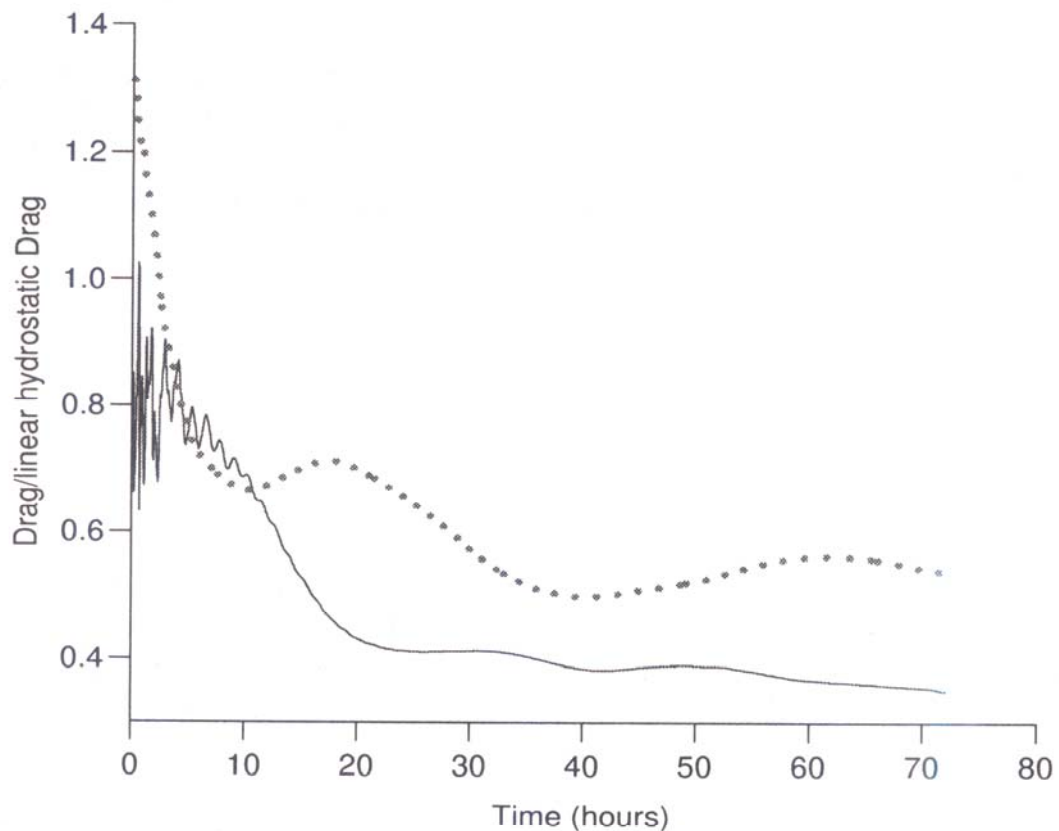


Fig. 12: Evolution of the normalised zonal component (continuous line) and the normalised meridional component (dotted line) of the surface pressure drag. Inviscid flow with background rotation. The Rossby number of the flow is 0.4. Integration time 72 hours.

Vorticity budget

A calculation of the different terms that contribute to the production of horizontal vorticity, equations (5) and (3), with the inclusion of background rotation shows that with the absence of viscous effects, that is $K = 0$ in equations (2) and (3) the baroclinic mechanism is the dominant source of horizontal vorticity.

Vertical structure of ζ

The intensity of ζ is found to decrease with height in a linear way from 300 metres up to 1200 metres after which height the decrease is much faster.

3.3 Third case study: Inviscid flow without background rotation

In this simulation both surface friction and background rotation have been removed. No explicit parametrisation of viscous effects has been included in the calculations and a free slip lower boundary condition has been used. Thus no vorticity is present in the upstream flow. Return flow in the lee of the orography is detected after an integration of 4 hours. The surface wind vectors are shown in Fig.13. This result corresponds to an integration of 12 hours. Two counter rotating vortices are observed in the lee of the orography. A calculation of the vertical vorticity ζ for a height of 400 metres and an integration of 12 hours is shown in Fig.14. Two well defined and symmetric areas of vorticity are found on the lee of the mountain. There is an area of anticyclonic vorticity located on the northern part of the wake and an area of cyclonic vorticity located on the southern part of the wake.

Since the upstream flow has no vorticity at all the vorticity observed in these calculations must be the result of the interaction between the flow and the obstacle. Smolarkiewicz and Rotunno

(1989) were the first to study the generation of vorticity in inviscid flows, they explained the generation of vorticity as been due to the creation of horizontal vorticity by a baroclinic mechanism and then the tilting of this horizontal vorticity in the vertical as the flow moves around the orography. They claimed that their results showed no evidence of the production of potential vorticity anomalies. Smith (1989) suggested that such anomalies ought to be produced in low-Froude number flow simulations, due to two main mechanisms:

- (a) lee-vortex formation by hydraulic jumps. At the hydraulic jump potential vorticity would be produced.
- (b) internal dissipation of the model.

As the model has a horizontal resolution that is constant in time, when the lee vortices are fully matured subgrid scale features have to be eliminated in order to avoid the onset of non-linear instability. This introduces dissipation in the simulation. At the start of the simulation no vorticity is present hence $\xi = \eta = \zeta = 0$ and horizontal vorticity can only be generated through the baroclinic terms, i.e., $\partial b'/\partial y$ and $\partial b'/\partial x$. Once horizontal vorticity has been created, vertical vorticity can be generated through the tilting of horizontal vorticity into the vertical. A computation of the vorticity budget after 12 hours of integration shows that the baroclinic terms are the main source of horizontal vorticity production.

A calculation of the potential vorticity at a height of 400 metres above level terrain for the parameters used here shows that although it is zero in the upstream flow it is not nil everywhere, this result can be seen in Fig.15. It can be seen that it has the same shape of the vorticity field shown in Fig.14.

The evolution of ζ and $PVnorm$ can be seen in Fig.16, in this case both quantities evolve together and it can be seen that $PVnorm$ is generated since the early stages of the integration.

The values of PV_{norm} and ζ zeta shown here correspond to the maximum values found on the northern vortex at a height of 400 metres above level terrain and the plot consists of 12 data points.

A simulation using the same parameter values used by Smolarkiewicz and Rotunno (1989) also yielded PV from the early stages of the calculations.

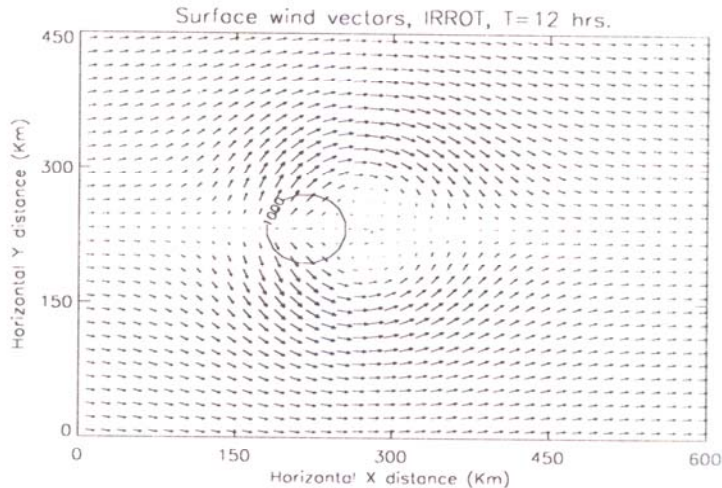


Fig. 13: Surface wind vectors obtained after an integration of 12 hours. Inviscid flow without background rotation. $F_r = 0.2$. The half-height contour is shown in order to indicate the location of the orography. Note that to scale the vectors the upstream flow is 4ms^{-1} .

REL. VORT. at Z=400M,T=12hrs,IRROT

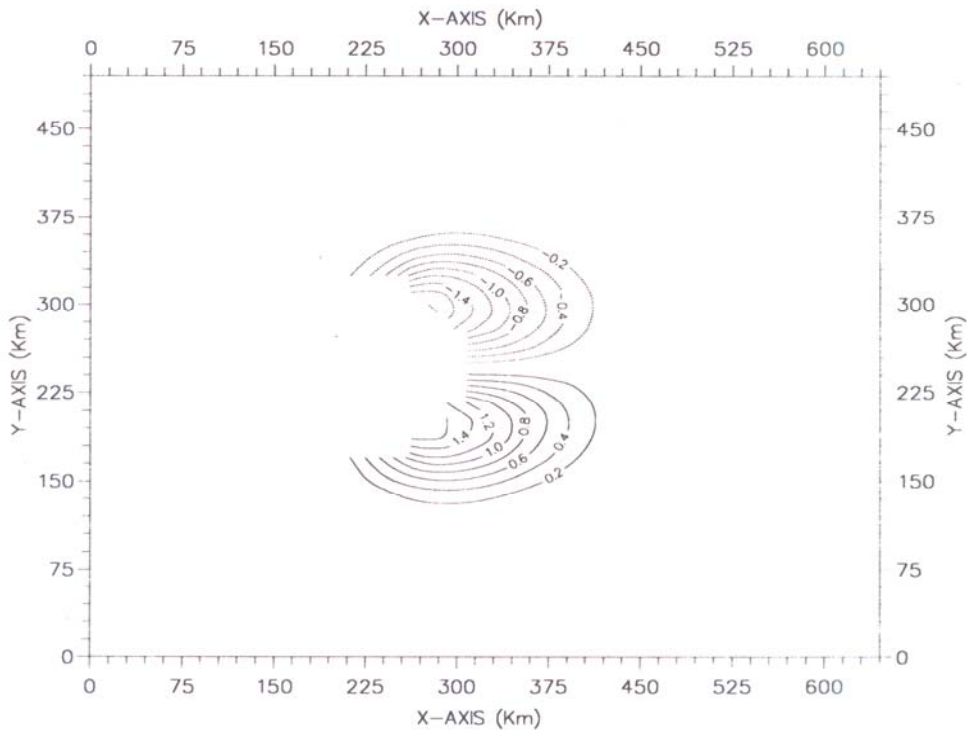


Fig. 14: Relative vorticity field at $z=400$ metres above level ground. Inviscid flow without background rotation. Integration time 12 hours. Contour interval $0.2 \times 10^{-4}\text{s}^{-1}$.

PV AT Z=400M,T=12hrs,IRROT

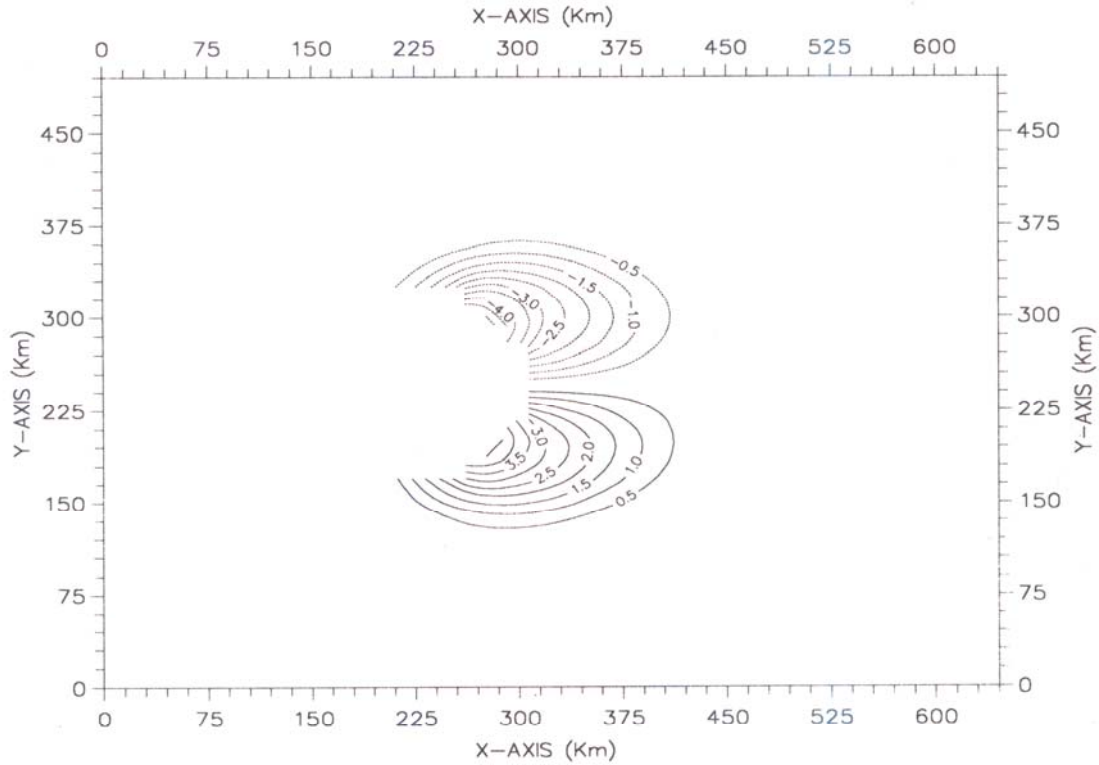


Fig 15: Potential vorticity field computed at 400 metres above level ground. Integration time 12 hours. Inviscid flow without background rotation. Contour interval $0.5 \times 10^{-7} \text{Kg}^{-1} \text{m}^2 \text{s}^{-1} \text{K}$.

Evolution of vorticity and PVnorm. Inviscid case without background rotation.

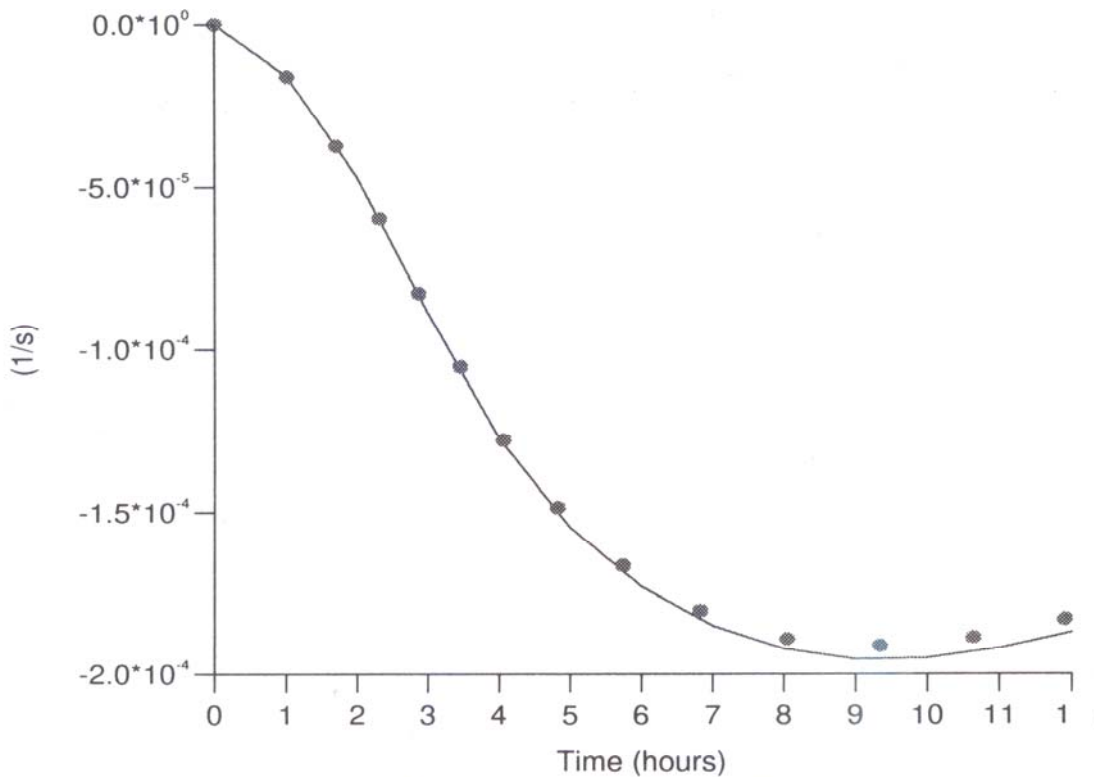


Fig. 16: Evolution of ζ and PV_{norm} . Inviscid flow without background rotation

The effects of a higher resolution on the evolution of PV_{norm} and ζ were investigated. To this effect the same orography, model domain, and initial flow profiles were used, the resolution chosen was three times higher than in the experiment without background rotation described in this section. No significant changes were found in either the evolution or the magnitudes of PV_{norm} and ζ . When an increase of a factor of 7.5 in the horizontal resolution was introduced it was found that the extrema of PV_{norm} and ζ were 4.5 times larger than their corresponding values found in the low resolution computations.

Vertical structure of ζ

The maximum of vorticity is located on the lee of the orography. The vorticity reaches a maximum at about 500 metres above level ground and begins to decrease in the vertical after that height. Almost no ζ is observed on the upwind side of the mountain, this is due to the fact that most of the production of vorticity due to tilting takes place at the flanks of the orography. A vertical profile of ζ taken at a point placed closed to the maximum of vorticity of the northern vortex shows that the intensity of ζ decreases almost linearly from 600 metres up to about 1500 metres and then it decreases almost exponentially beyond this point.

4. Conclusions

The production of vorticity and potential vorticity in the case of a uniform stratified flow over and around an isolated bell-shaped mountain with a circular base is studied. The effects of background rotation and surface friction have been considered. The Froude number chosen for these simulations is 0.2.

A comparison of the relative contributions to the total vorticity budget is made. It is found that in the absence of background rotation and

shear and using a free-slip lower boundary condition for inviscid flow the baroclinic mechanism is the main source of horizontal vorticity. This horizontal vorticity is tilted into the vertical and generates two counter-rotating lee-vortices. Introducing rotation shows that the baroclinic mechanism remains an important source of horizontal vorticity but it is closely followed by additional tilting terms which depend on the Coriolis parameter. The simulations of viscous flow where a no-slip boundary condition was used yield the important result that the baroclinic term is then not an important contributor to the horizontal vorticity budget. Other terms in the vorticity equation are about seven times larger than the baroclinic term.

The vertical structure of the vertical component of vorticity has a very different shape for each of these cases. For inviscid flow without background rotation the maximum of relative vertical vorticity is found on the lee of the mountain. The vertical vorticity decreases with height. Only small vertical vorticity is found on the upwind side of the orography. Including rotation it is found that the maximum of vertical vorticity is then located on the lee of the orography and that the vertical vorticity field in this area is weaker than in the case without background rotation. Areas of positive and negative values of relative vertical vorticity are found on the upwind side of the orography. These are due to stretching and then contraction of the vortex tube created by the background vorticity as the isentropes first separate and then contract as they approach the mountain.

The simulations of viscous flow show that the maximum of vorticity is again located on the lee slope of the mountain, but this zone 'rotates' with height inside the boundary layer. The vertical vorticity field has a much smaller vertical extension than in the previous two cases. This is due to the fact that most of the vorticity is generated within the boundary layer. Much larger values of relative vertical vorticity are found on the upwind side of the orography than in any of the

other two cases studied. This is due to the tilting of the horizontal vortex tubes created by the no-slip boundary condition.

The rate of production of potential vorticity has been computed. There are two areas where potential vorticity is produced, negative potential vorticity on the northern flank of the orography and positive potential vorticity on the southern flank of the mountain (flow is from the west and assumes to be in the Northern Hemisphere).

A quantity called normalised potential vorticity is defined to allow the relation between the vorticity and potential vorticity produced to be quantified. The evolution of normalised potential vorticity is such that it is produced since the early stages of the integration for both the non-rotating and the rotating inviscid flows. This is due to the implicit diffusion implied by using a numerical method. It is important to stress that we believe that (any) numerical model has to include such diffusion. It would appear to be extremely difficult to find a potential vorticity conserving numerical scheme in the context of a non-hydrostatic model integrating the momentum and thermodynamic equations. Given that frictional effects produce more anomalous potential vorticity than that due to the implicit numerical diffusion it perhaps remains as an academic question as to how to carry out a genuinely inviscid numerical calculation.

This evolution of normalised potential vorticity is also studied for a viscous flow and it is observed that more normalised potential vorticity is produced in this case as expected due to the inclusion of friction.

The onset of vortex shedding due to the introduction of asymmetries in the flow is also studied. The asymmetries in the flow were introduced by including background rotation in the simulation, this creates an asymmetry in the upwind flow and allows the vortex eddies to be shed.

Acknowledgements

We wish to thank Dr. M. Athanassiadou for useful comments. The first author wishes to acknowledge the help of the World Meteorological Organisation, the Finnish Meteorological Office and the Universidad de Costa Rica in the form of grants that allowed him to pursue this research.

RESUMEN

En estudios anteriores se ha postulado que los vórtices observados en el sotavento de montañas con dimensiones de mesoescala pueden deberse a una variedad de interacciones del flujo en el barlovento de la montaña, entre ellos, la producción inviscida baroclínica de vorticidad, la influencia de la rotación de la Tierra y procesos viscosos en la capa límite.

En este artículo se examina cuantitativamente la importancia relativa de estos tres mecanismos para un flujo con estabilidad estática constante que pasa sobre y alrededor de una montaña aislada con dimensiones tales que el número de Rossby es 0.4 y el número de Froude es 0.2. Una capa límite de Ekman es empleada en las simulaciones en las que el papel de la fricción es investigado. El presupuesto completo de vorticidad es evaluado y de esta manera pueden identificarse las principales fuentes de vorticidad por medio de simulaciones numéricas hechas con un modelo tridimensional y no hidrostático. Se encuentra que cuando se incluye una capa límite los vórtices se forman en los flancos de la orografía debido a mecanismos viscosos. El mecanismo baroclínico (inviscido) está presente pero constituye una pequeña contribución al presupuesto de la vorticidad horizontal. La asimetría introducida por la rotación de la Tierra acentúa la tendencia al arrastre de vórtices en el sotavento de la montaña.

Los efectos de la fricción también generan vorticidad potencial, aunque debe emplearse cautela al analizar el presupuesto de la vorticidad potencial ya que existe una fuente debida a la disipación numérica inherente en el modelo usado, así como en cualquier otro modelo de mesoescala. Esta fuente implícita de vorticidad potencial dificulta la interpretación de la dinámica de las supuestas simulaciones inviscidas en términos de la vorticidad potencial. Para este tipo de problemas el uso del análisis de la dinámica del flujo por medio de la vorticidad es menos ambiguo que el análisis por medio de la vorticidad potencial.

En experimentos sin rotación, sin fricción, con un flujo cuyo perfil de velocidad es uniforme y con una condición de frontera de libre deslizamiento se encuentra que el mecanismo baroclínico es la principal fuente de vorticidad horizontal. Esta es proyectada en la vertical generando así dos vórtices en el sotavento de la orografía. Cuando se incluye rotación en el sistema de coordenadas el mecanismo baroclínico sigue siendo una fuente importante de vorticidad pero los términos de proyección (tilting) generan vorticidad del mismo orden de magnitud. Cuando se simula un flujo viscoso sujeto a una condición de no deslizamiento el término baroclínico ya no es dominante en la producción de vorticidad en la horizontal.

Se ha definido una nueva cantidad llamada vorticidad potencial normalizada, con ella se investiga la relación entre la producción de vorticidad y la producción de la vorticidad potencial.

Se encuentra que la vorticidad potencial normalizada se produce desde temprano en la simulación en todos los casos investigados. La vorticidad potencial normalizada obtenida en los experimentos sin viscosidad es debida a la difusión implícita del modelo. En el caso del fluido viscoso mas vorticidad potencial normalizada es generada que en los experimentos inviscidos debido a la parametrización explícita de la difusión.

Para un viento oeste en el hemisferio norte se produce vorticidad potencial negativa en el flanco norte de la orografía y vorticidad potencial positiva en el flanco sur. También se ha investigado la relación entre el arrastre de vórtices y la presencia de asimetrías en el flujo. Las asimetrías fueron introducidas en el flujo al añadir rotación al sistema de coordenadas.

References

- Boyer, D., P. Davies, W. Holland, F. Biolley, H. Honji, 1987. Stratified rotating flow over and around isolated three-dimensional topography. *Phil. Trans. R. Soc. Lond.*, **A322**, 213-241.
- Brighton, P., 1978. Strongly stratified flow past three-dimensional obstacles. *Q. J. Roy. Met. Soc.*, **104**, 289-307.
- Chopra, K., and L. Hubert, 1965. Mesoscale eddies in the wake of islands. *Journal of the Atmospheric Sciences*, **22**, 652-657
- Etling, D., 1989. On atmospheric vortex streets in the wake of large islands. *Meteorology Atmos. Physics*, **41**, 157-164.
- Grubisic, V., and R. B. Smith and C. Schär, 1995. The effects of bottom friction on shallow-water flow past an isolated obstacle. *Journal of the Atmospheric Sciences*, **52**, No 11, 1985-2005.
- Jensen, N. and E. Agee, 1978. Vortex cloud street during AMTEX 75. *Tellus*, **30**, 517-523
- Lettau, H. H., 1939. *Atmosphärische Turbulenz*. Leipzig: Akad. Verlag, 283 pp.
- Miranda, P.M.A. and I. N. James, 1992. Non-linear three-dimensional effects on gravity-wave drag: Splitting flow and breaking waves. *Q. J. Roy. Met. Soc.*, **118**, 1057-1081.
- Schär, C. and R.B. Smith, 1993. Shallow-water flow past isolated topography. Part II: Transition to vortex shedding. *Journal of the Atmospheric Sciences*, **50**, No 10, 1401-1412.
- Schär, C. and D.R. Durran, 1996. Vortex formation and vortex shedding in continuously stratified flows past isolated topography. Submitted to *Journal of the Atmospheric Sciences*.
- Smith, R. B., 1989. Comment on low Froude number flow past three-dimensional obstacles Part I: Baroclinically generated lee vortices. *Journal of the Atmospheric Sciences*, **46**, No 23, 3611-3613.
- Smith, R. B., and V. Grubisic, 1993. Aerial observations of Hawaii's wake. *Journal of the Atmospheric Sciences*, **50**, No 22, 3729-3750
- Smolarkiewicz, P. K. and R. Rotunno, 1989. Low Froude number flow past isolated topography. Part I: Baroclinically generated lee vortices. *Journal of the Atmospheric Sciences*, **46**, 1154-1164.
- Sun, W. and J. Chern, 1994. Numerical experiments of vortices in the wake of large idealized islands. *Journal of the Atmospheric Sciences*, **51**, No 2, 191-209.
- Thorpe, A., H. Volkert, and D. Heinmann, 1993. Potential vorticity of flow over the Alps. *Journal of the Atmospheric Sciences*, **50**, 1573-1590.
- Trischka, J., 1980. Cone models of mountain peaks associated with atmospheric vortices. *Tellus*, **32**, 365-375.

